






## Labrador Sea Water Formation Rate and Its Impact on the Local Meridional Overturning Circulation

Charlène Feucher<sup>1</sup> , Yarisbel Garcia-Quintana<sup>1</sup> , Igor Yashayaev<sup>2</sup> , Xianmin Hu<sup>1,2</sup> ,  
 and Paul G. Myers<sup>1</sup> 

<sup>1</sup>Department of Earth and Atmospheric Sciences, University of Alberta, Edmonton, Alberta, Canada, <sup>2</sup>Bedford Institute of Oceanography, Fisheries and Oceans Canada, Dartmouth, Nova Scotia, Canada

### Key Points:

- Strong convection events in the Labrador Sea entail a high formation rate of Labrador Sea Water
- Part of the Labrador Sea Water is exported out of its formation region through the Deep Western Boundary Current within 1 year
- Strong, deep convection events are related to a higher local MOC index in the Labrador Sea along the AR7W section

### Correspondence to:

C. Feucher,  
 feucher@ualberta.ca

### Citation:

Feucher, C. E., Garcia-Quintana, Y., Yashayaev, I., Hu, X., & Myers, P. G. (2019). Labrador Sea Water formation rate and its impact on the local Meridional Overturning Circulation. *Journal of Geophysical Research: Oceans*, 124, 5654–5670. <https://doi.org/10.1029/2019JC015065>

Received 18 FEB 2019

Accepted 17 JUL 2019

Accepted article online 24 JUL 2019

Published online 13 AUG 2019

**Abstract** This paper investigates the link between the Labrador Sea Water (LSW) formation rate and the strength of the Atlantic Meridional Overturning Circulation within the Labrador Sea. LSW is formed in the Labrador Sea through deep wintertime ocean convection and is then carried out of the basin by, among other currents, the Deep Western Boundary Current (DWBC) that flows southward along the east coast of Canada. We used an eddy-permitting simulation (at 1/12°, horizontal resolution) with an Arctic and Northern Hemisphere Atlantic configuration of the Nucleus for European Modeling of the Ocean (NEMO) model that covers the period from 2002 to 2017. In this study, the formation rate of LSW is estimated using an instantaneous kinematic subduction approach by analyzing the vertical transport of a water mass through the base of the mixed layer. We computed the local Meridional Overturning Circulation (MOC) index and the transport of LSW within the DWBC at the Atlantic Repeat hydrographic section 7 West (AR7W). Results show that an increase in the formation rate of LSW entails an increase in the LSW transport in the DWBC within 1 year. This is followed by an enhancement of the overturning in the Labrador Sea.

**Plain Language Summary** The Atlantic Meridional Overturning Circulation (AMOC) is of paramount importance for the climate. The AMOC contributes to the redistribution of heat, salt, and anthropogenic carbon in the world's oceans. The upper limb of the AMOC transports warm, surface water northward. The lower limb of the AMOC is associated with dense, cold, and deep water formation and is carried by a vigorous Deep Western Boundary Current (DWBC). The Labrador Sea Water (LSW) is one of the water masses formed by deep convection in the subpolar gyre and then carried out of the basin by, among other currents, the DWBC that flows southward along the east coast of Canada. In this paper, we use a simulation to investigate how the change in the formation rate of the LSW could impact the strength of the local AMOC in the Labrador Sea. We found that an increase in the formation rate of LSW entails an increase in the LSW transport in the DWBC within 1 year. This is followed by an enhancement of the overturning in the Labrador Sea.

### 1. Introduction

The Meridional Overturning Circulation (MOC) is a crucial component of the Earth's climate system. The MOC redistributes heat, freshwater, salt, nutrients, and gases, including anthropogenic carbon between the upper and deep layers of the world's oceans. The MOC is governed by densification of waters at high latitudes. In the Atlantic Ocean, wintertime cooling drives the MOC, which advects warm and salty surface waters from subtropical latitudes to high northern latitudes. A primary location for this mixing of Atlantic waters, with fresher polar waters and their conversion to cold, fresh and dense waters, is the Labrador Sea. The main features of the subpolar North Atlantic Ocean are shown in Figure 1, adapted from Daniault et al. (2016).

The Labrador Sea is the main site for deep convection in the North Atlantic Ocean (Dickson et al., 1996), and is where the Labrador Sea Water (LSW) is formed (Clarke & Gascard, 1983). During and following its formation through convective mixing of unusually high (extreme) heat losses, LSW tends to fill a specific intermediate-depth layer over most of the deep basin, while also being injected into the large-scale mid-depth to deep circulation system via the Deep Western Boundary Current (DWBC; Dickson & Brown, 1994). Several other pathways spread LSW across the North Atlantic basins (e.g., Rhein et al., 2011; Yashayaev

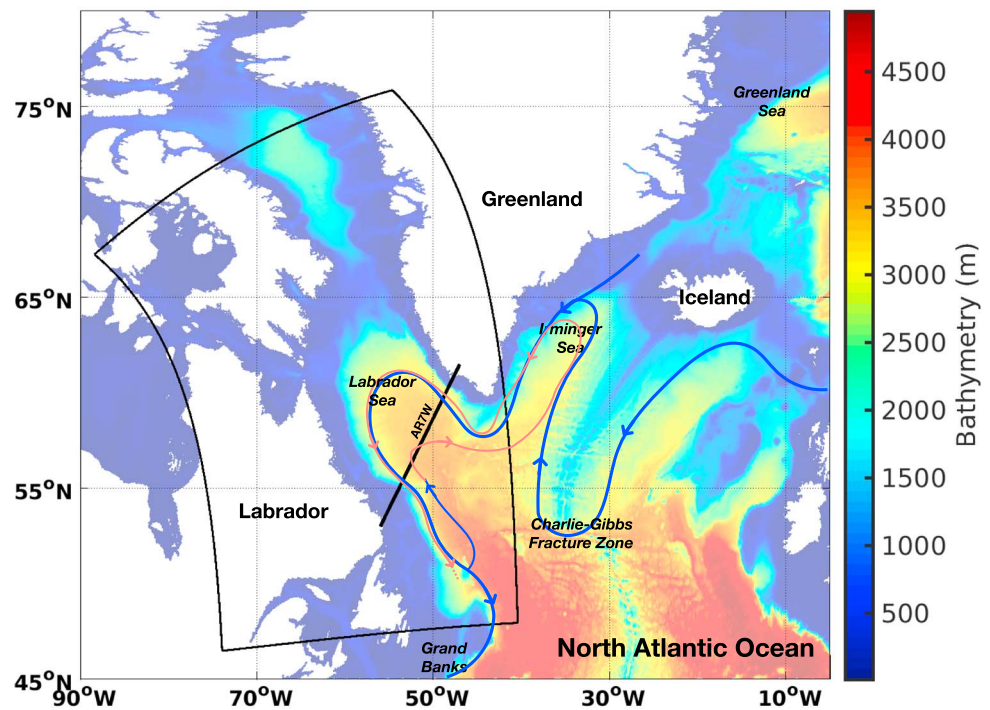


**Figure 1.** Map focusing on a part of the subpolar gyre in the North Atlantic Ocean, showing the Labrador, Irminger, and Greenland Seas. Color shading represents the bathymetry (in meters). The study area including the Labrador Sea is represented by the black rectangle. The location of the AR7W section is indicated by the black line. Schematic large-scale circulation is based on Danialt et al. (2016): deep and cold currents including the Deep Western Boundary Currents (blue path) and intermediate currents of Labrador Sea Water (orange path). AR7W = Atlantic Repeat hydrographic section 7 West.

& Loder, 2016; 2017). The DWBC constitutes the lower limb of the MOC (Hirschi & Marotzke, 2007) and advects newly formed deep and bottom waters southward to the subtropics (Pickart et al., 1997).

Over the last decades, the DWBC has been widely studied, often by means of recurrent moored measurements at 53°N (Zantopp et al., 2017). The vertical and horizontal structure of the DWBC system is very complex, and its spatial and temporal variability have a direct impact on the MOC. The DWBC spreads over a broad depth range between 400 and 4000 m with a volume transport likely varying between about 10 and 40 Sv depending on location (Dengler et al., 2004; Toole et al., 2011, 2017).

Changes in the deep water formation rate directly affect the ventilation of the deep ocean and hence the ocean's ability and potential to absorb and store anthropogenic carbon (Rhein et al., 2017), as well as the strength of the MOC and the associated heat transport (Kieke & Yashayaev, 2015). Häkkinen and Rhines (2004) have suggested that there could be a cessation of deep convection in the Labrador Sea and the thermohaline circulation in the Atlantic Ocean. Many numerical studies also confirmed a link between the LSW formation rate and the strength of the Atlantic Meridional Overturning Circulation (AMOC; e.g., Kuhlbrodt et al., 2007). Böning et al. (2006) found a link between the DWBC and the intensity of the convection in the Labrador Sea. Using a simple measure of LSW formation, they discovered that stronger southward transport episodes were notably associated with convection events, convection leading with a lag of 1 to 2 years.

Yashayaev and Loder (2016, 2017) have demonstrated that the properties of LSW, including its thickness anomaly, propagate across the entire subpolar North Atlantic in 5 to 7 years confirming connectivity of key water properties of the deep layers of the North Atlantic and those of the source water masses. Thornalley et al. (2018) have recently shown that the LSW density representing the strength of convective overturning in the Labrador Sea, and the strength of the DWBC along the North American continental slope as far as Cape Hatteras, are significantly correlated on decadal and longer timescales. Thornalley et al., 2018's (2018) result is based on proxies rather than direct measurements: The changes in the strength of the DWBC were reconstructed from sortable-silt sediment grain size data. The fact that larger grain sizes are associated with stronger currents and smaller sizes with weaker currents allows them to use the sediment core data

as a natural long-term current meter monitoring the strength on the major ocean arteries. On seasonal to interannual scales, the amount of LSW injected into the regions outside the Labrador Sea was found to be proportional to the volume of LSW produced each year (Yashayaev & Loder, 2016).

However, there are some alternative views on the essence and strength of the relationship between convection and overturning in the North Atlantic (Böning et al., 2006; Lozier et al., 2012, 2016; Marsh et al., 2005; Mauritzen & Häkkinen, 1999; Pickart & Spall, 2007; Straneo, 2006). Many of these studies have suggested a link between the formation of the LSW and the AMOC. However, no conclusive observational evidence for a link between dense water formation in the Labrador Sea and AMOC variability has emerged to date. The link between dense water formation in the Labrador Sea and AMOC variability is still under debate (Li & Lozier, 2018; Lozier et al., 2012, 2019; Thornalley et al., 2018). A major problem is that the estimation of the local AMOC—in the subpolar gyre—is mostly based on spring-summer data. But, according to Yashayaev and Loder (2016), there is a strong seasonal variation in the LSW volume and hence in the local AMOC. The values based on ship data conducted once a year, normally in spring-summer, are then likely to underestimate the LSW production rate and its contribution to local AMOC. Thus, the present estimates undermine the relationship between the formation rate of LSW and the AMOC. Even the studies that agree with such a connection underestimate this relationship.

Such a broad range of results and opinions calls for an in-depth analysis of connectivity between various characteristics of the pools of water homogenized by winter convection each year and the amounts of water injected in the same or following years into the DWBC. Motivated by this need, we investigate the relationship between the formation rate of the LSW and the strength of the local MOC in the Labrador Sea. In our analyses, we use a simulation from the Nucleus for European Modeling of the Ocean (NEMO) numerical framework, and a method of analysis of 4-D density fields, which was previously used to analyze the Argo and shipboard observations in the same region. To analyze the formation rates and related dynamics of any convectively formed water mass and particularly LSW, we propose here an approach based on a kinematic subduction approach quantifying the vertical transport of water masses through the base of the mixed layer. We accurately define the LSW density range based on the analysis of the subduction rate in the deep convection region. The relationship between the formation of LSW and the transport in the DWBC is then investigated to understand how the change in the LSW formation rate could impact the strength of the local MOC in the Labrador Sea. Our present study provides the first insights of how the formation rate of the LSW could impact the strength of the local MOC in the Labrador Sea.

The article is organized as follows: Section 2 describes the NEMO simulation, as well as the methods used to define the deep convection region, and the kinematic subduction approach used to define the LSW density range and LSW formation rate. Results are presented in section 3: spatial and temporal variability of the deep convection region, density range of LSW and volume of newly formed LSW based on potential vorticity and density criteria, LSW formation rate, relationship between LSW formation rate, DWBC current transport and the local MOC at the AR7W section. Results are discussed in section 4. Conclusions are drawn in section 5.

## 2. Data and Method

### 2.1. The NEMO Simulation

In this study, the numerical simulation uses a coupled ocean and sea ice system based on the NEMO (available at <https://www.nemo-ocean.eu>) version 3.4 (Madec, 2008). The sea ice model used here is the Louvain-la-Neuve sea Ice Model version 2 with an elastic-viscous-plastic rheology (Hunke & Dukowicz, 1997), including both thermodynamic and dynamic components (Bouillon et al., 2009; Fichefet & Morales Maqueda, 1997). Freshwater fluxes from Greenland (liquid component only) with a spatial resolution of 5 km are based on Bamber et al. (2012). More detailed setup of the ocean and sea ice component can be found in Hu et al. (2018) and Grivault et al. (2018). The regional configuration ANHA12 covers the Arctic Ocean and the Northern Hemisphere Atlantic with a horizontal resolution of  $1/12^\circ$  (Grivault et al., 2018; Hu et al., 2018). In the study area (Labrador Sea), it reaches a resolution of 5 to 6 km. There are two open boundaries, one close to Bering Strait in the Pacific Ocean and the other one at  $20^\circ\text{S}$  across the Atlantic Ocean. The vertical grid contains 50 levels with layer thickness smoothly increasing from 1 m at the surface level to 458 m in the last level. High resolution is applied to the upper ocean, that is, 22 levels for the top 100 m. Partial step is also enabled to better resolve the sea floor (Barnier et al., 2006). The simulation is integrated from 1 January 2002 to 31 December 2017. Initial conditions, including three-dimensional (3-D) ocean fields (temperature,

salinity, zonal velocity, and meridional velocity) as well as two-dimensional (2-D) sea surface height and sea ice fields (concentration and thickness) are interpolated from the 1/4° Global Ocean Reanalysis and Simulations (GLORYS2v3) produced by Mercator Ocean (Masina et al., 2015). The monthly open boundary conditions (temperature, salinity, and horizontal ocean velocities) are also extracted from GLORYS2v3 product. At the surface, it is driven with high temporal (hourly) and spatial resolution (33 km) atmospheric forcing data from the Canadian Meteorological Centre Global Deterministic Prediction System ReForecasts data set (Smith et al., 2014), including 10-m winds, 2-m air temperature and specific humidity, shortwave and longwave radiation fluxes, and total precipitation. Our analyses are based on 5-day-average outputs for the period ranging from January 2002 to December 2017. However, the first few years of the simulation are impacted by the adjustment to the initial conditions from GLORYS and are excluded from the interpretation of our present results. We thus performed our analyses using data from the 2005–2017 period.

## 2.2. Method: Defining the LSW Density Range

The newly formed LSW is defined uniquely for each year on a short period. This definition on actual properties of a targeted water mass may significantly change from year to year in response to varying atmospheric forcing, upper ocean salinity, and even history of previous convective events and their signature in ocean heat and freshwater content and stratification (Yashayaev, 2007; Yashayaev & Loder, 2009, 2016, 2017; Yashayaev, van Aken, et al., 2007, Yashayaev, Bersch, et al., 2007). The versions of LSW defined by this approach are often grouped into classes. The definition of such LSW year classes can be based on volumetric analysis of density (e.g., Yashayaev, 2007; Yashayaev & Loder, 2016; Yashayaev, van Aken, et al., 2007), or/and temperature and salinity (e.g., Yashayaev & Loder, 2017). This approach provides a framework for studying the physical properties of water masses, their variability, mixing, dynamics, and transport. In the present study, we will extend the volumetric approach to define LSW in model simulations and demonstrate its effectiveness for linking convection and local MOC in the Labrador Sea.

There are two main reasons for using this approach—the volumetric year-class method—to define an intermittently formed water mass for analyzing, studying, and interpreting model solutions (results of model runs). The first reason is specific to ocean models and descends from the fact that LSW is typically/usually saltier and therefore denser in the analyzed model simulations than in the observations. In particular, LSW simulated by the ANHA12 configuration is 0.03 kg/m<sup>3</sup> denser than recently observed. This higher density is due to a drift in the salinity field that increases the density of seawater in the simulation. Rattan et al. (2010) showed that large salinity drift occurring in the Labrador Sea led to excessive and unrealistic convection in simulations and hence overestimated LSW formation rates. The second reason for using the volumetric year-class method in model studies is that the density range of newly formed LSW can vary significantly from year to year depending on the conditions controlling winter convection in the Labrador Sea: air-sea fluxes, vertical stratification, freshwater flux, and other factors. As shown in the recent studies from Yashayaev and Loder (2016, 2017), variability in the strength and depth of convection entails a seasonal and interannual change in the hydrographic properties, volume, and export of LSW formed.

We determine the density range of LSW for each year by modifying this method for the present study. This allows a change in the hydrographic properties of the newly formed LSW in response to changes in the atmospheric and oceanic conditions that control convective mixing. In addition to finding the active LSW density range with the volumetric method, we determine the density range through computation and analysis of the subduction rate. We describe below the full method used.

The kinematic subduction approach has been used to quantify the transfer of water from the mixed layer to the stratified thermocline (Cushman-Roisin, 1987; Marshall et al., 1993; Williams, 2001). We adapted this method to the case of water mass subduction in the Labrador Sea. By quantifying the water mass subduction rate and analyzing it as a function of density, we determined the density range of LSW formed each year, complementing the volumetric class approach. The kinematic subduction approach considers the vertical transport of a water mass through the base of the instantaneous mixed layer. This approach is detailed in Courtois et al. (2018). We briefly summarize the method here. The subduction rate  $S$  is defined as follows:

$$S(\sigma_h) = -\frac{1}{\tau} \int_0^\tau \int_{A_\sigma} \left[ w_b + \frac{\partial h}{\partial t} + v \cdot \nabla h \right] dA_\sigma dt, \quad (1)$$

where  $w_b$  is the vertical velocity at the base of the mixed layer (interpolated from vertical velocity model outputs),  $\frac{\partial h}{\partial t}$  represents the rate of change of depth of the instantaneous mixed layer, and  $v \cdot \nabla h$  represents

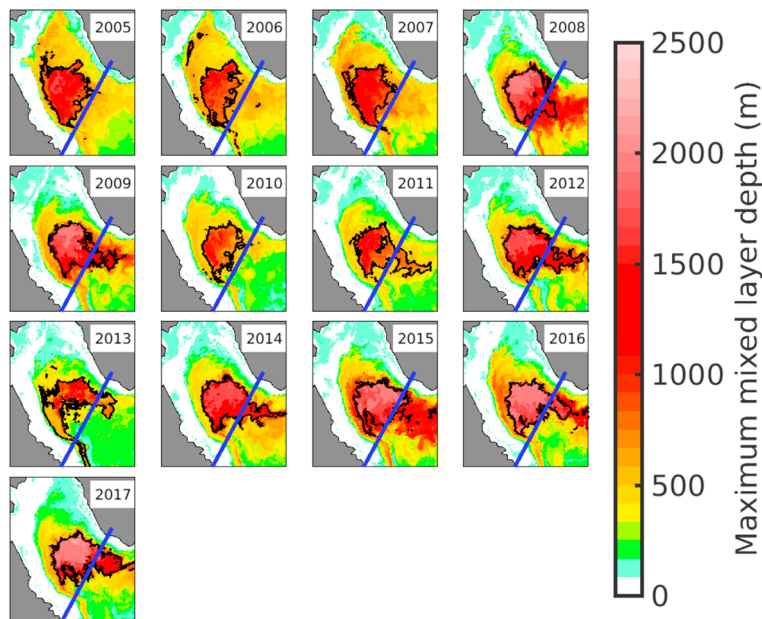


**Figure 2.** Defining the deep convection region in the Labrador Sea. Color shading indicates the maximum mixed layer depth of the year (January to December, in meters). Black contours highlight the area of the 90th percentiles of the deepest mixed layers and delineate the deep convection region. The blue line indicates the location of the Atlantic Repeat hydrographic section 7 West section (AR7W).

the advective terms crossing horizontally the sloped base of the mixed layer.  $A_\sigma$  is the outcrop area defined as  $A_\sigma(t) = [x : \sigma_1 \leq \sigma_h(x, t) \leq \sigma_1 + \delta\sigma_1]$ , with  $\sigma_h$  the instantaneous mixed layer density;  $\tau$  is the time period of integration. Note that we use potential density  $\sigma_1$  referenced to 1,000 m. In equation (1), subduction processes are positive ( $S > 0$ ), and obduction processes are negative ( $S < 0$ ).

To determine the LSW density range, we computed the subduction rate  $S$  within the deep convection region where LSW is formed. The deep convection region is defined as follows: At every grid point within the Labrador Sea, we determined the maximum mixed layer depth (MLD) for each year, from January to December. We then delineated the region of deep convection for every year by taking the 90th percentiles of these deepest mixed layers. The MLD is computed using the algorithm described in Courtois et al. (2017), which is a new approach, to determine the MLD in deep convection for numerical models.

### 3. Results

#### 3.1. Winter Convection in the Labrador Sea

Figure 2 shows the resulting contours that delineate the deep convection region for each year. The convection averaged-depth in the deep convection region is shown Figure 3. In general, the deep convection region is centered in the basin, but its extension slightly varies from year to year (Figure 2). Deep convection is known to occur locally in the southwest part of the Labrador Sea (e.g., Holte & Straneo, 2017). The extension area of deep convection in our simulation is more extensive than in the observations. The model resolution could be influencing the results on convection area (Böning et al., 2016; Chanut et al., 2008). Energetics Irminger rings generated of the West Greenland and Irminger current off Cape Desolation play a role in the heat budget of the Central Labrador Sea, and thus in the convection. These Irminger rings, which are not properly represented with  $1/12^\circ$  (e.g., Chanut et al., 2008), would otherwise provide buoyancy to cap and reduce convection in the northern part of the domain. In 2011, 2012, 2014, 2016, and 2017, the deep convection region extends up to the southern tip of the Greenland Coast, which is realistic with regard to observations (Fröb et al., 2016; Yashayaev & Loder, 2016; 2017) and is also recurrent in ocean models (Rattan et al., 2010).

In 2006 and 2007, the deep convection region is restricted on the western side but continues to feed the DWBC, suggesting interannual changes in the distribution of outflowing LSW between its different pathways. In 2013, the deep convection region is dramatically reduced to a nearly peripheral shape of its average spatial extent. It extends, however, as far southwest and east along the respective boundaries as in any

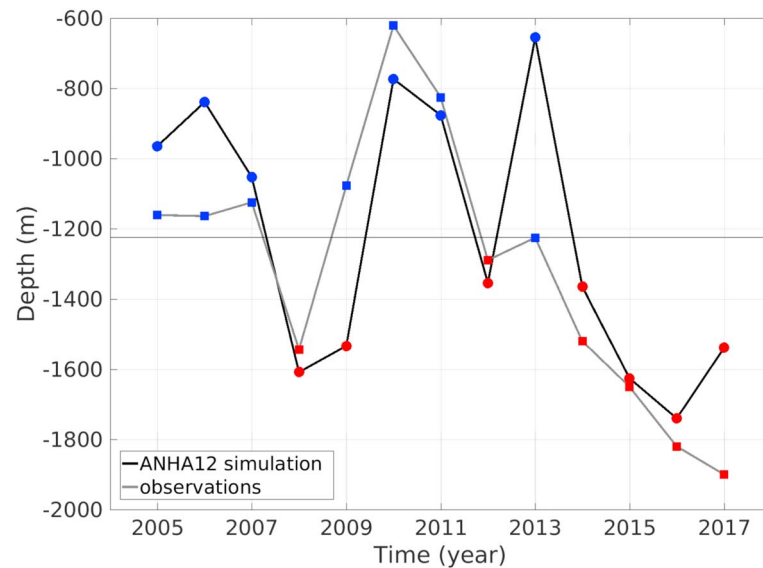


**Figure 3.** Depth of the convection (in meters). Black curve: simulated depth of the convection averaged in the deep convection region as delineated by contours Figure 2. Gray curve: observed depth of the convection as indicated in Yashayaev and Loder (2016). Blue (red) dots (squares for the observations, circles for the simulation) highlight years of weak (strong) convection and relatively shallow (deep) mixed layer. The horizontal black line represents the mean depth of the deep convection in the ANHA12 simulation (1225 m).

year of strong convection. The average maximum depth of the deep convection exhibits a strong interannual variability (Figure 3; ; Holte & Straneo, 2017; Yashayaev & Loder, 2017). The depth of the convection varies between 600 m for the shallowest mixed layers and 1,800 m for the deepest mixed layers. From 2014 to 2017, the depth of the convection increases from 1,365 to 1,740 m, which is the maximum depth over the period studied. In our simulation, very deep convection events are also observed in 2008 with a depth reaching 1,608 m, and in 2012 with a depth reaching 1,355 m. The weak convection event that occurs in 2013 has a depth reaching 655 m. Two other weak convection events also occur in 2006 with a depth of 839 m, and in 2010 with a depth of 773.5 m. To summarize, 2008, 2009, 2012, and 2014–2017 are years with relatively strong convection (red dots in Figure 3) and 2005–2007, 2010, 2011, and 2013 are years with relatively weak convection (blue dots in Figure 3), using a value of 1,225 m (mean value of the depth of the convection in the simulation represented by the black line in Figure 3) for the aggregate maximum convection depths as the threshold. The magnitude of the deep convection in the simulation is consistent with the observations (Yashayaev & Loder, 2016, 2017). We compare the estimates of maximum convection depth with those compiled by Yashayaev and Loder (2016, 2017) and updated for this investigation. The Argo and ship survey profiles are used to delineate the depth of maximal development of convection for each year. The percentile-based computation of maximum MLD is discussed in Yashayaev and Loder (2016). Here we note that, just as in the model, the deep convection events are strong in 2008, 2012, and 2014–2017, and low in 2005–2007, 2010, and 2011. In 2013, there is a discrepancy between the model and the observations: the MLD is much shallower in the model (655 m) than in the observations (1,200 m). The reason for disagreement could be the preconditioning and/or the overall shallow and small deep convection region observed in the model in 2013 (Figure 3). For preconditioning, the model may not be capable, as of today, to retain LSW for long. The ocean has a better memory than the model, which we call interconvection preconditioning or post-convection preconditioning (Yashayaev & Loder, 2017), with mixing deepening while heat losses decreased in 2016. As shown in Figure 3, this trend continued in 2017, when heat losses were not strong. The same thing could have happened in 2013, because 2012 convection was strong not only in the Labrador Sea, but in the Irminger Sea providing a massive wide spread preconditioning for 2013.

### 3.2. LSW Density Range and Volume

We computed the subduction rate within the deep convection region to define the density range of LSW for each year. Subduction rate  $S$  is integrated in the time-varying region of deep convection (see Figure 2), from April to September (equation (1)).

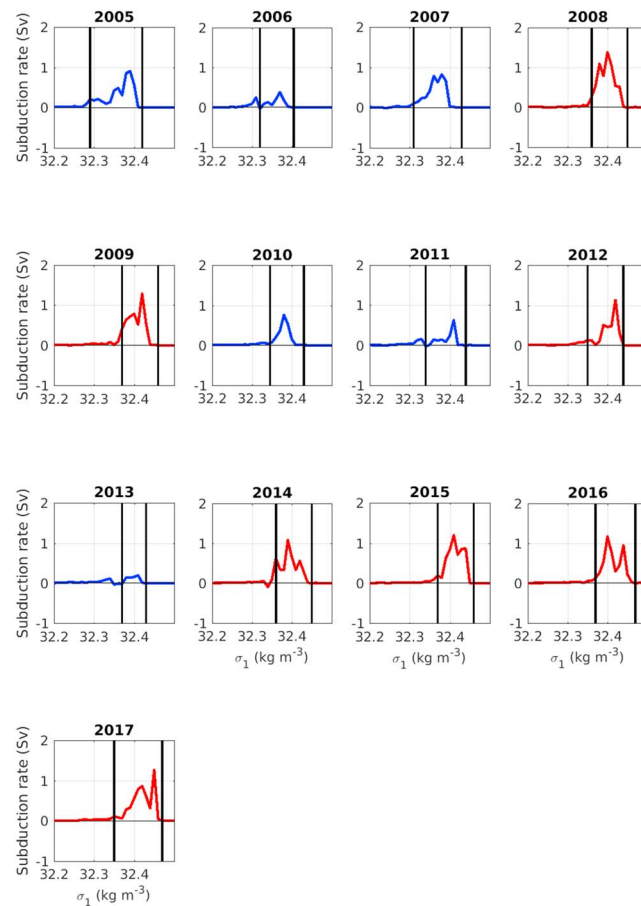


**Figure 4.** Annual mean subduction rate  $S$  in sverdrup as a function of the potential density  $\sigma_1$  (referenced to 1,000 m) and integrated in the time-varying region of deep convection (Figure 3) from April to September. Density range of Labrador Sea Water is defined for each year and is delineated by the two vertical black lines around the maximum subduction rate.

During this period, the LSW subducts below the mixed layer ( $S > 0$ ) and is exported out of its formation region (Straneo et al., 2003; Zou & Lozier, 2016). We thus expect to accurately track the density range of LSW formed at that moment. Figure 4 shows the subduction rate for each year, as a function of the potential density  $\sigma_1$  from 32.2 to 32.5  $\text{kg/m}^3$ . The highest subduction rate is reached in 2008 with 1.39 Sv (at density  $\sigma_1 = 32.40$ ), and the lowest is reached in 2013 with 0.20 Sv (at density  $\sigma_1 = 32.41$ ). On average, the maximum subduction rate is about  $0.94 \text{ Sv} \pm 0.37 \text{ Sv}$ . The maximum occurs around the density of  $\sigma_1 = 32.40 \pm 0.02 \text{ kg/m}^3$ . Two low values in the subduction rate are reached in 2006 (0.38 Sv at density  $\sigma_1 = 32.37 \text{ kg/m}^3$ ), and 2011 (0.63 Sv at density  $\sigma_1 = 32.41 \text{ kg/m}^3$ ). High values of subduction rate are also reached in 2012 (1.15 Sv at density  $\sigma_1 = 32.42 \text{ kg/m}^3$ ) and over the last years of the simulation: 1.08 (at density  $\sigma_1 = 32.39$ ) in 2014, 1.19 (at density  $\sigma_1 = 32.41 \text{ kg/m}^3$ ) in 2015, 1.16 (at density  $\sigma_1 = 32.40 \text{ kg/m}^3$ ) in 2016, and 1.26 (at density  $\sigma_1 = 32.45 \text{ kg/m}^3$ ) in 2017. In general, higher subduction rate is associated with higher density around the maximum.

We defined the density range of newly formed LSW by taking the density range for which the subduction rate is strictly superior to zero around the maximum subduction rate. Black vertical lines in Figure 4 delineate the density range of the LSW formed during the corresponding year. We observe a strong variability in the density range of the newly formed LSW; the trend is to increase with time. As mentioned previously, this trend is due to the bias in salinity. The density for the lower limit of LSW range increases from  $\sigma_1 = 32.29 \text{ kg/m}^3$  in 2005 to  $\sigma_1 = 32.35 \text{ kg/m}^3$  in 2017. The density for the upper limit of LSW range increases from  $\sigma_1 = 32.42 \text{ kg/m}^3$  in 2005 to  $\sigma_1 = 32.47 \text{ kg/m}^3$  in 2017. The mean density of upper limit of LSW range is  $\sigma_1 = 32.44 \pm 0.02 \text{ kg/m}^3$  and  $\sigma_1 = 32.35 \pm 0.03 \text{ kg/m}^3$  for the lower limit. In 2016, there is a maximum density for the upper and lower limits:  $\sigma_1 = 32.47 \text{ kg/m}^3$  and  $\sigma_1 = 32.37 \text{ kg/m}^3$ , respectively. In 2009, LSW also

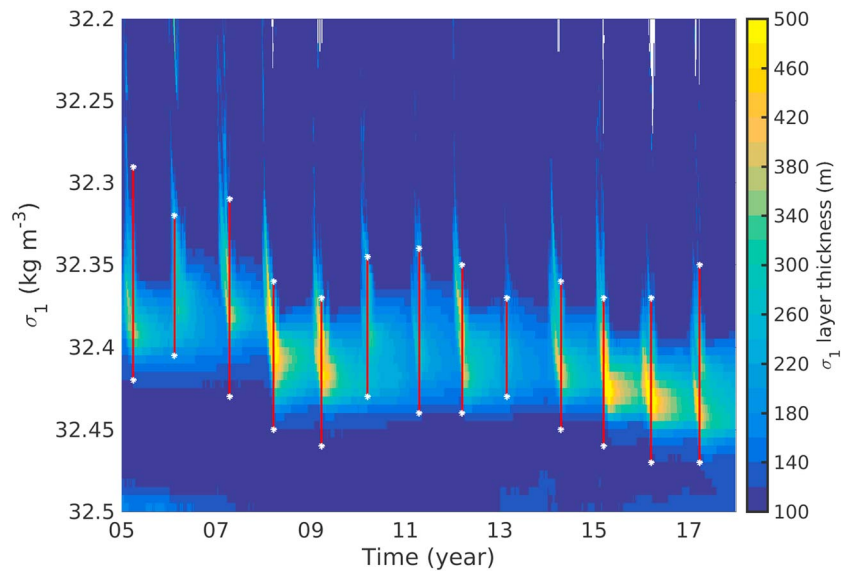


**Figure 5.** Time-density display of potential density  $\sigma_1$  layer thickness ( $\sigma_1 \pm 0.0025$ , in meters) averaged in the time-varying region of deep convection (Figure 3). Red lines highlight the Labrador Sea Water layer as identified using subduction rate analyses (Figure 4).

exhibits high densities for its lower and upper limits:  $\sigma_1 = 32.46 \text{ kg/m}^3$  and  $\sigma_1 = 32.37 \text{ kg/m}^3$ , respectively. The density range of LSW in our results is higher than in the observations. Yashayaev and Loder (2016) using Argo data found that density of LSW varies between  $\sigma_1 = 32.33 \text{ kg/m}^3$  to  $\sigma_1 = 32.37 \text{ kg/m}^3$ .

The spanning density range of LSW also significantly varies from year to year. It is lowest in 2013, with a spanning density range of  $0.06 \text{ kg/m}^3$ , and it is highest in 2005 and in 2007, with a spanning density range of  $0.13 \text{ kg/m}^3$ . In 2011, a large spanning density range is also observed and equal to  $0.10 \text{ kg/m}^3$ . From 2014 to 2015, the spanning density range is  $0.09 \text{ kg/m}^3$ . From 2008 to 2010, a low spanning density range is observed and equal to  $0.09 \text{ kg/m}^3$ . From 2015 to 2017, the spanning range increases from  $0.09$  to  $0.12 \text{ kg/m}^3$ .

Following Yashayaev and Loder (2016, 2017), we performed a density layer analysis within the deep convection region to validate the definition of the LSW in our simulation. Figure 5 shows the  $\sigma_1$  layer thickness ( $\sigma_1 \pm 0.0025 \text{ kg/m}^3$ ) averaged over the time-varying deep convection region. The thicker part on the histogram, between 380 and 500 m, highlights the LSW layer. We see the increasing density trend of LSW over time. High subduction rate of LSW is related to thicker LSW (as observed in 2008, 2009, 2012 and from 2014 to 2017; Figure 4), while the lower formation of LSW is related to thinner LSW (as observed in 2006 and 2013; Figure 4). The largest  $\sigma_1$  layer thickness are 615 m in 2008, 461 m in 2012, 585 m in 2015, 536 m in 2016, and 478 m in 2017. In 2013, the largest  $\sigma_1$  layer thickness is 250 m, and it is 329 m in 2006. The amplitude of  $\sigma_1$  layer thickness and their variability is consistent with what is observed. In a previous study, Yashayaev and Loder (2016) found that  $\sigma_1$  layer thickness in the LSW varies between 300 m and up to 590 m in 2014 and 2016. They also found a very thick and dense LSW from 2014 to 2016, respectively. Dense and thick LSW found in 2008 is also well reproduced in the simulation.

The density range of LSW computed from the subduction rate analysis (Figure 4) falls into the thickest part of the histogram (Figure 5) and delineates well the LSW layer. This finding allows us to validate the density range found to define LSW for each year.

### 3.3. LSW Formation

Figure 6 shows the subduction rate  $S$  computed over the Labrador Sea (the studied area for the Labrador Sea is shown Figure 1), accumulated over the yearly LSW density classes and integrated during the restratification period ( $\tau$  from April to September,  $S > 0$ ; see equation (1)). We expect that the method used to compute the subduction rate reflects the formation rate of LSW. To validate this hypothesis, we also compute the volume of newly formed LSW based on potential vorticity criteria (Li & Lozier, 2018; Talley & McCartney, 1982; Zou & Lozier, 2016). We computed the volume of newly formed LSW over the Labrador Sea. For



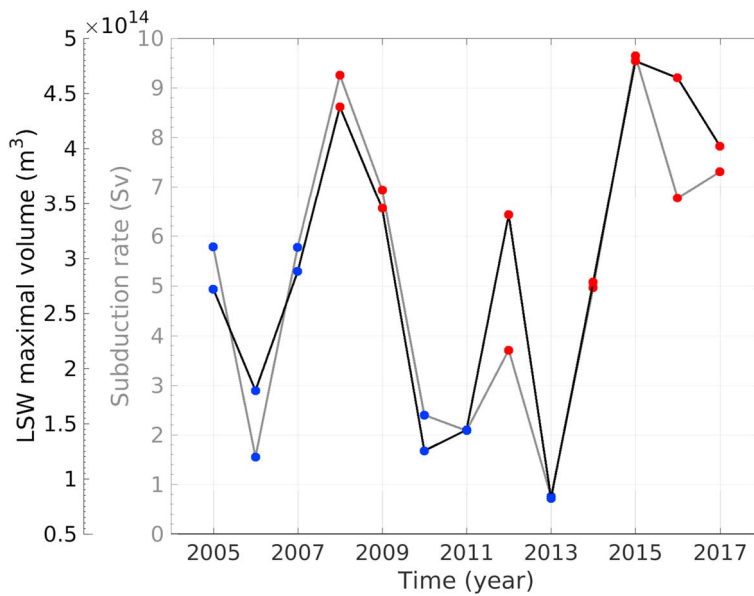


**Figure 6.** Net subduction rate cumulated over the density range of LSW (gray curve, Sv), and winter maximum volume of newly formed LSW (black curve, m<sup>3</sup>) computed in the Labrador Sea (area defining the Labrador Sea is shown Figure 2). Blue (red) dots highlight years of weak (strong) convection and relatively shallow (deep) mixed layer. LSW = Labrador Sea Water.

our calculation of newly formed LSW, we used both potential vorticity  $q$  and the density constraint to define this water mass. Assuming relative vorticity is small compared to planetary vorticity, potential vorticity  $q$  is defined as follows:

$$q = -\frac{f}{\sigma} \frac{\partial \sigma}{\partial z}, \quad (2)$$

where  $f$  is the Coriolis parameter and  $\sigma$  is the potential density. In the simulation, newly formed LSW is defined as the water mass in the density range defined previously for each year, with  $q < 4 \times 10^{-12} \text{ m}^{-1} \cdot \text{s}^{-1}$ . We used the same potential vorticity threshold used by Talley and McCartney (1982). The volume of newly formed LSW is calculated as follows. First, the gridded density fields are searched to find all grids that satisfied the density and potential vorticity constraints discussed above. The volume of all grids that meet these constraints is summed to yield the total volume of newly formed LSW in the Labrador Sea for every 5 days. Then we determined the maximum volume of newly formed LSW every year. We found that the maximum volume of newly formed LSW is reached in March and April.

Figure 6 shows the variability of LSW subduction rate and newly formed LSW maximum volume. There is a good agreement between the two parameters, which allows us to validate our hypothesis: LSW subduction rate reflects well the formation rate of LSW. The correlation between LSW subduction rate and the maximum volume of newly formed LSW is 0.9 at zero lag. The maximal LSW volume is on average  $2.95 \times 10^{14} \pm 1.32 \times 10^{14} \text{ m}^3$ . LSW subduction rate is on average  $5.15 \pm 2.88 \text{ Sv}$ . Newly formed LSW reaches its minimum volume in 2013 ( $0.8 \times 10^{14} \text{ m}^3$ ), while the subduction rate is also the smallest with 0.8 Sv. Maximum volume is reached in 2015 with a volume of  $5.0 \times 10^{14} \text{ m}^3$  and a subduction rate of 9.64 Sv. In 2008, high LSW volume and the highest subduction rate are observed: 9.26 Sv maximum subduction rate with a winter maximum volume of  $4.38 \times 10^{14} \text{ m}^3$ . In 2012, subduction rate is 3.71 Sv and maximum volume is  $3.39 \times 10^{14} \text{ m}^3$ . In 2006, there is a low subduction rate (1.55 Sv) and a low maximum volume ( $1.80 \times 10^{14} \text{ m}^3$ ).

In general, high volume and high subduction rate are associated with enhanced deep convection. Comparing the magnitude of the deep convection (Figure 3) with LSW subduction rate and maximum volume (Figure 6), we notice that the observed strong convection events in 2008, 2012, and from 2014 to 2017 are associated with high subduction rate and maximum volume. On the contrary, the weak convection events observed 2006, 2010, and 2013 are associated with a small LSW subduction rate and volume.

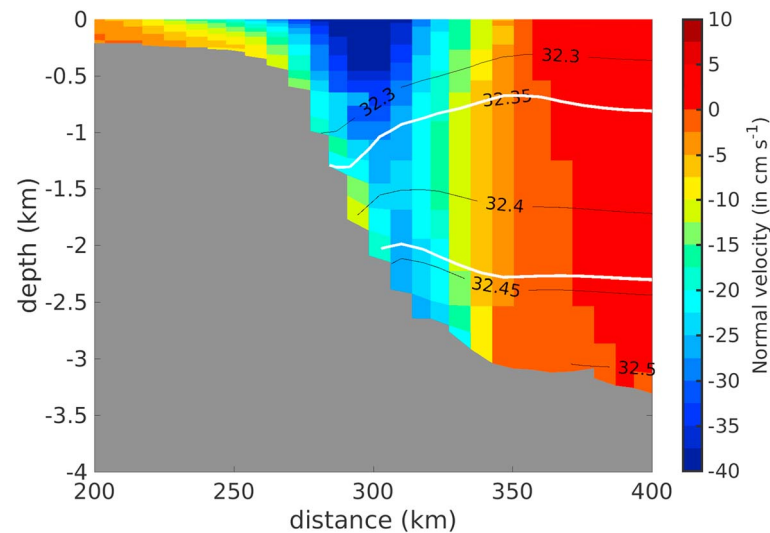


**Figure 7.** Mean meridional velocity (2005–2017, cm/s) at the Atlantic Repeat hydrographic section 7 West in the vicinity of the Western Boundary Current. Contours represent the mean density field  $\sigma_1$ . White contours delineates the Labrador Sea Water layer as formed in 2012.

### 3.4. LSW Formation Rate and DWBC

We now explore the correlation between the formation rate of LSW and its transport in the DWBC. We aim to understand if an increase in the subduction rate of LSW entails an increase in LSW transport in the DWBC. Figure 7 shows the mean model velocity in the vicinity of the WBC across the AR7W section (cm/s; averaged over the 2005–2017 period, velocities are negative southward). Strong southward velocities highlight the core of the WBC that is intensified in the surface. The structure and magnitude of the velocities in the WBC are well reproduced by the simulation. Maximum velocities are found in the surface with values of 35 cm/s. They decrease with depth where values are around 20 cm/s. These values are consistent with observations at 53°N (e.g., Böning et al., 2006; Handmann et al., 2018; Zantopp et al., 2017). Black contours in Figure 7 represent the mean potential density  $\sigma_1$  field (averaged over the 2005–2017 period), while white contours delineate the LSW formed in 2012. LSW is found in the layer between 1,000- and 2,500-meter depth, which is consistent with observations. This layer of LSW partially or entirely overlaps with a broader defined deep LSW (Zantopp et al., 2017).

We computed the LSW volume transport as the sum of the southward transport of water between the bounding isopycnals defining the LSW at the AR7W section and potential vorticity  $q < 4 \times 10^{-12} \text{ m}^{-1} \cdot \text{s}^{-1}$ . We also considered the different LSW density range, and we calculated the monthly LSW transport along the DWBC with a 0-year lag (Straneo et al., 2003; Zou & Lozier, 2016). The LSW transport in the DWBC at 0-year lag means that when computing the transport during a given year, we use the density range of LSW of the same year.

Figure 8 shows the monthly LSW transport at AR7W in the DWBC (red curve). The LSW transport with a 0-year lag is stronger in spring, with a maximum value of 5.8 Sv in March 2006. High values are reached in 2007 (5.3 Sv), in 2008 (3.5 Sv), and at the end of the period studied (3.3 Sv in 2015 and 4.8 Sv in 2016). In 2013, LSW transport is nearly zero: The criteria defining the LSW layer are not met in the boundary current at AR7W (density range and potential vorticity). In 2013, the convection depth/region is very weak (Figure 3), and the formation rate of LSW is very low (Figure 4). The variability of the LSW transport compares well with the formation rate of LSW. The high formation rate of LSW corresponds to a highest LSW transport in the DWBC. The magnitude of the LSW transport in the DWBC is underestimated when comparing with observations. Zantopp et al. (2017) found a LSW transport in the DWBC at 53°N varies between 10 and 20 Sv from 1997 to 2015. In another study, Böning et al. (2006) found a mean transport of 14.5 Sv in the deep LSW density range in the DWBC at 53°N (average over the 1992–2002 period). Note that the method we used to compute LSW transport in the DWBC is different from the one used in the papers as mentioned above (i.e., we used a specific LSW density range and potential vorticity constraint), as well as a location that is further north.

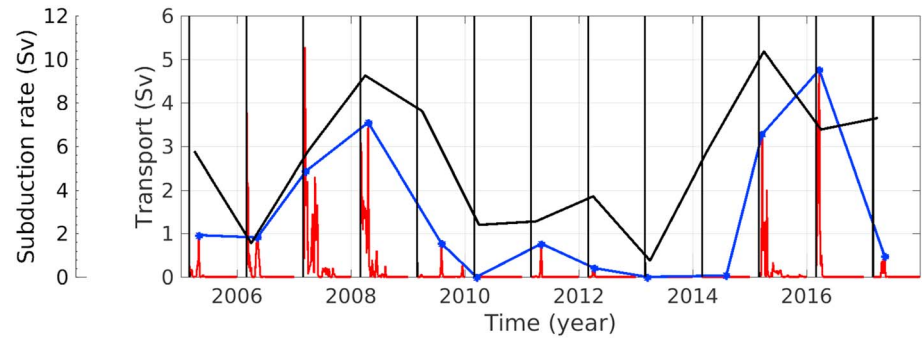


**Figure 8.** Monthly LSW transport in the Western Boundary Current at Atlantic Repeat hydrographic section 7 West at 0-year lag (red curve, Sv), maximum LSW transport (from March to December, blue curve, Sv), and net subduction rate cumulated over the density range of LSW (black curve, Sv). Vertical black lines are drawn every 1 March. LSW = Labrador Sea Water.

Figure 8 also shows the maximum LSW transport for each year in the DWBC at AR7W (from March to December, blue curve). The maximum LSW transport increases from 2006 (1.0 Sv) to 2008 (3.5 Sv) and then an overall decrease from 2008 to 2013, where it is 0 Sv. From 2014, the LSW maximum transport increases up to 4.7 Sv in 2016, which is a year of very strong convection.

### 3.5. LSW Formation Rate and MOC

Finally, we investigate the link between the LSW formation rate and the strength of the local MOC in the Labrador Sea (referred as  $MOC_{west}$  in the following). We aim to understand if the LSW formation rate is associated with a higher  $MOC_{west}$  index.

The  $MOC_{west}$  index is computed at the AR7W section and is defined as the maximum of the overturning stream function in density  $\sigma_1$  space:

$$MOC_{west}(t) = \arg \max_{\sigma_1} \left( \int_{\sigma_1}^0 \int_{x_e}^{x_w} (v - T_{net}) d\sigma_1 dz \right), \quad (3)$$

where  $v$  are the velocities normal to the AR7W section. Velocities  $v$  are integrated from west ( $x_w$ ) to east ( $x_e$ ) and from top to bottom across density surface  $\sigma_1$ .  $T_{net}$  represents the net transport across the AR7W section:

$$T_{net} = \frac{\int_x \int_z v dA}{\int_x \int_z dA}, \quad (4)$$

where  $A$  is the area of the AR7W section. The net transport is removed from the full velocity field before calculating the  $MOC_{west}$  index, such that the resulting  $MOC_{west}$  values are associated with zeros net mass transport (e.g., McCarthy et al., 2015). We then computed the monthly mean value of the  $MOC_{west}$ .

Figure 9 shows the maximum values (from March to December) of the  $MOC_{west}$  at AR7W from 2005 to 2017 (standardized, black curve). The mean  $MOC_{west}$  index at AR7W is  $5.8 \pm 1.6$  Sv for the 2005–2017 period. Pickart and Spall (2007) measured the  $MOC_{west}$  in density space in summer at AR7W and found a mean value of 2 Sv. Recently, Lozier et al. (2019) measured the  $MOC_{west}$  across OSNAP west in density space and found a mean value of  $2.1 \pm 0.3$  Sv over the period August 2014 to April 2016. These values differ from our results. These discrepancies could be because vessel data are for spring-summer and do not have sufficient resolution to avoid smearing strong boundary currents. Seasonal and interannual changes in volume (Yashayaev & Loder, 2016, 2017) are not included in the OSNAP estimate (Lozier et al., 2019). Moorings may not have sufficient vertical resolutions, and density measurements may not be accurate enough to follow changes in layer thickness.

The maximum values of the  $MOC_{west}$  index exhibit a strong variability (Figure 9). We observe two trends: A first period when the  $MOC_{west}$  decreases by 2.5 Sv from 2007 to 2011, and then a second period from 2011 to 2016 when the  $MOC_{west}$  increases by 2.7 Sv. Over the period studied, there are two local maxima observed in 2009 and 2012. There are also three local minima observed in 2008, 2013, and 2017.

Figure 9 also compares the annual subduction rate of LSW (red curve), the maximum  $MOC_{west}$  index (black curve), and the maximum transport of LSW in the DWBC (blue curve). Over the 2005–2017 period, the

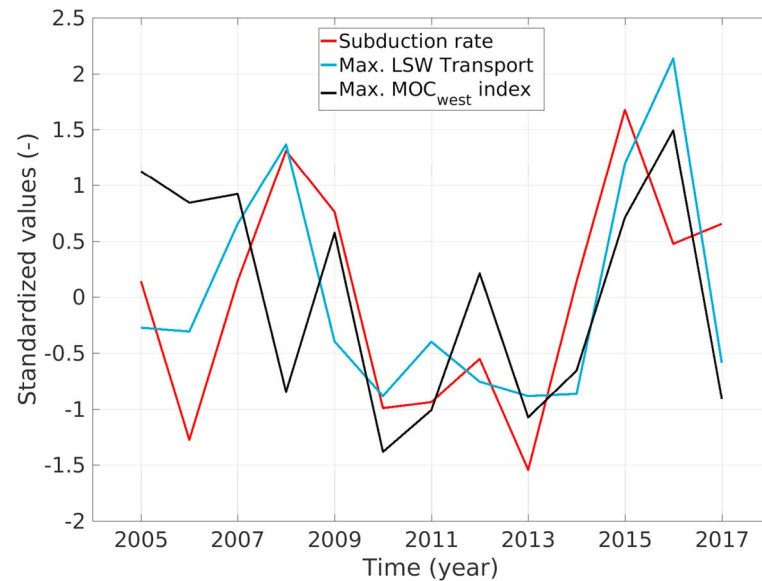


**Figure 9.** Net subduction rate cumulated over the density range of LSW (red curve, Sv), maximum LSW transport at 0-year lag (blue curve, Sv), and maximum  $MOC_{west}$  index computed at the Atlantic Repeat hydrographic section 7 West section (black curve, in Sv). LSW = Labrador Sea Water; MOC = Meridional Overturning Circulation.

LSW subduction rate and LSW transport exhibit similar variability. The correlation is 0.6 at 0 lag and with a level of confidence of 90%. When comparing the maximum  $MOC_{west}$  index with the other two variables, we observe that the  $MOC_{west}$  index exhibits similar variability only from 2009. The first 5 years show a different variability. From 2005 to 2007, while the maximum LSW transport in the DWBC at AR7W and the LSW subduction rate exhibit a minimum, the maximum  $MOC_{west}$  index exhibits a maximum. From 2007 to 2009, this trend is reversed. We thus decide to compute the correlation from 2009 to 2017. The correlation between the maximum LSW transport in the DWBC at AR7W and the maximum  $MOC_{west}$  index is 0.8 with 0 lag and is significant at a 99% level. The correlation between the LSW subduction rate and the maximum  $MOC_{west}$  index is 0.7 with 0 lag, and it is significant at a 95% level. The correlation between the LSW subduction rate and the LSW transport in the DWBC at AR7W is 0.6 with 0 lag, and it is significant at a 90% level. Therefore, with regard to these correlations, we find that an increase in the subduction rate of LSW increases the transport in the DWBC and then the  $MOC_{west}$  index is enhanced within one year. These correlations have to be taken carefully, given the short period studied.

#### 4. Discussion

We investigated the relationship between the LSW formation rate, the LSW transport in the DWBC at AR7W, and the overturning in the Labrador Sea. We found that an increase in the formation rate of LSW entails an increase in the LSW transport in the DWBC and then enhances the local overturning.

We used an innovative approach to quantify the formation rate of the LSW. We used an instantaneous kinematic subduction approach by analyzing the vertical transport of a water mass through the base of the mixed layer. Using this method, we have been able to determine accurately the subduction or formation rate of LSW, as well as the density range of LSW formed each year. Our results from the LSW formation rate compare well with the quantification of the volume of newly formed LSW, which allows us to validate the analysis of the LSW formation rate using this kinematic subduction approach. However, given the known model salinity drift, it is possible the density of the LSW produced in the model is too large, which might also lead to overestimations in the water formation rates.

We found that the newly formed LSW is exported out of its formation region and increases the LSW transport in the DWBC at AR7W: the more dense water formed, the more it gets exported. Studies show that it takes about a year for a large volume of LSW to shift to the Irminger Sea (Yashayaev, 2007; Yashayaev, van Aken, et al., 2007; Yashayaev, Bersch, et al., 2007). To better understand how the LSW could impact the transport of the DWBC, we analyzed the path of the LSW using an offline Lagrangian tool, ARIANE (Blanke & Raynaud,

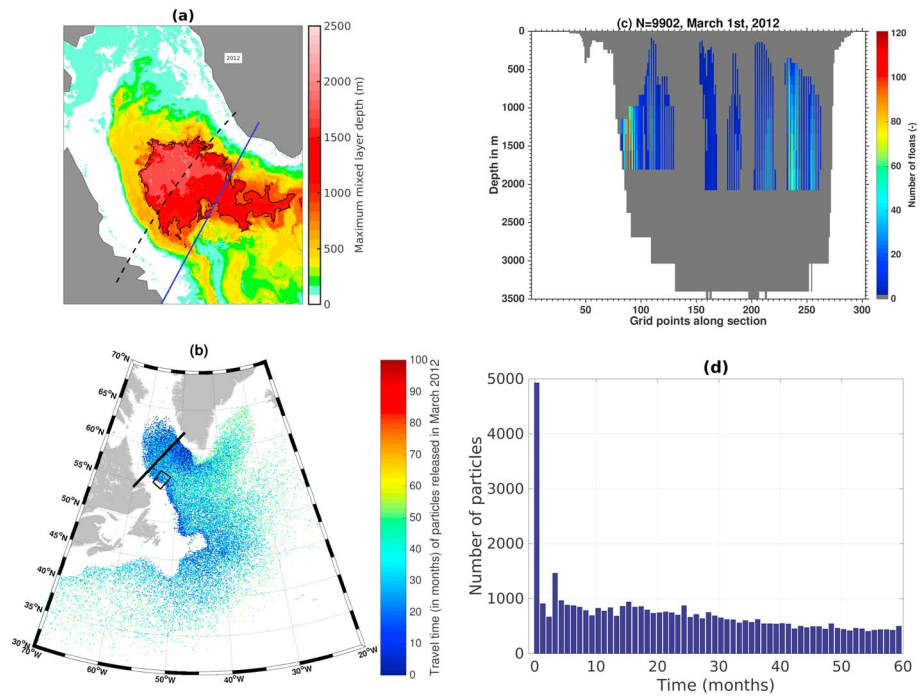


**Figure 10.** (a) Location of the section where ARIANE virtual floats are launched. Color shading indicates the maximum mixed layer depth in 2012 (January to December, in meters). Contours highlight the area of deepest mixed layers and delineate the deep convection region in 2012. The blue line indicates the location of the AR7W section. (b) Distribution of the virtual floats launched on 1 March 2012 along the section (indicated by the dashed curve in panel a). Virtual floats are distributed along the section where the density of the particles fall into the density range of Labrador Sea Water formed in 2012 and if the particles are going southward normal to the section. (c) The travel time of the virtual floats released on 1 March 2012 (month). (d) The number of virtual floats found in the AR7W section as a function of their travel time (month). Virtual floats are counted within the box centered in the Western Boundary Current at the AR7W section and shown in (b). AR7W = Atlantic Repeat hydrographic section 7 West.

1997; Blanke et al., 1999). ARIANE is a well-known tool to explore the large-scale ocean circulation. This diagnostic allows us to quantitatively and qualitatively track water volumes associated with a particular water mass (e.g., Blanke et al., 2002). We computed three-dimensional (3-D) trajectories using ARIANE from ocean velocity field. Virtual floats are launched early winter (1 March of every year) within the density range of LSW formed in that corresponding year. We then tracked the LSW and analyzed its path. Figure 10 shows the location of the section where the virtual floats are launched (dashed curve). This section is taken upstream of the AR7W section. We aim to know how long it takes for the virtual floats to reach the AR7W section. To illustrate our analyses, we chose to present the results from ARIANE using the virtual floats launched in 2012, a year for which a strong and deep convection occurred.

Figure 10a shows the distribution of the virtual floats as of 1 March 2012. Nine thousand nine hundred two virtual floats were launched that year. Virtual floats are distributed along the section shown in Figure 10a following two constraints: (1) density of the particle has to fall into the density range of LSW formed in 2012 and (2) normal velocity along the section of the particles has to be southward. We observe in Figure 10b that the virtual floats are mostly confined to the DWBC, where velocities are southward. Up to 120 virtual floats can be found in this western part of the section. The rest of the virtual floats are located in the center of the section and in the eastern region where velocities are also southward.

Figure 10c shows the travel time of the virtual floats released on 1 March 2012, integrated up to December 2017. The travel time is found between 0 and 4 years (0 and 50 months). After its formation, in less than 1 year, LSW spreads all over the center of the Labrador Sea. Then, there are two paths where LSW is quickly exported from its formation region in less than one year. The first path is along the DWBC and the Gulf Stream, which transport LSW into the North Atlantic subtropical gyre (Fischer & Schott, 2002; Lavender et al., 2000; Straneo et al., 2003). The second path is along the eastern boundary current that transports LSW into the Irminger Sea (Piron et al., 2016).

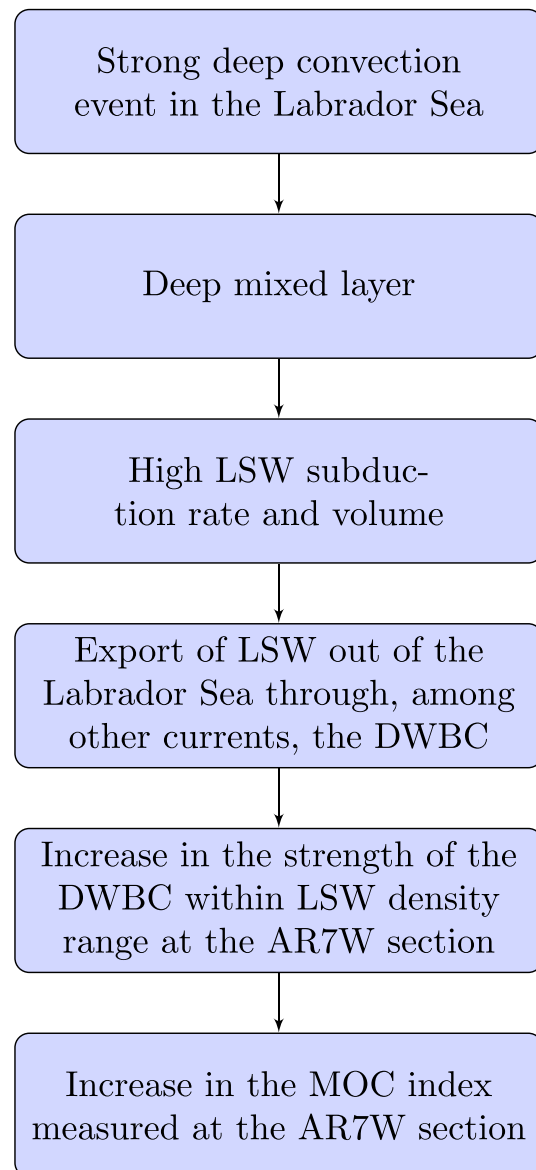


**Figure 11.** Flow chart summarizing the main findings of the present study. AR7W = Atlantic Repeat hydrographic section 7 West; LSW = Labrador Sea Water; DWBC = Deep Western Boundary Current; MOC = Meridional Overturning Circulation.

Figure 10d shows the number of virtual floats found in the AR7W section as a function of their travel time (month). Virtual floats are counted within the box centered in the DWBC at the AR7W section and shown Figure 10c. From the 9,902 virtual floats launched, 4,927 virtual floats are found in the DWBC at the AR7W section within the first month. These results support well the correlation we found, showing that the LSW transport in the DWBC increases within one year after the formation and export of the LSW.

## 5. Conclusion

In this study, we investigated the relationship between the formation rate of the LSW and the overturning in the Labrador Sea. Our results based on the analyses of a realistic simulation reveal that there are good relationships between these two quantities. Our main findings are (Figure 11): (1) Within 1 year after its formation, the LSW is almost instantaneously exported out of its formation region, mostly through the DWBC, which then increases the LSW transport in the DWBC at AR7W, and (2) the LSW transport in the DWBC is

correlated with the  $MOC_{west}$  index at the AR7W with 0 lag, which means that there is enhancement in the local overturning in the Labrador Sea.

This study is based on the use of a model. Each model has limitations and certain advantages over other models. A truly comprehensive model-based diagnosis of convection and its impact on AMOC and ocean circulation in general can be achieved by expanding the concepts and method introduced and developed in our study by applying the same procedures to other models and performing side-by-side comparisons of model performance in reproduction of convection, LSW formation, seasonal evolution, export, and impact on the AMOC. The NEMO simulation we use has a realistic physics of heat exchange and general ocean dynamics, so the results we discuss are in agreement with observations and real-world or real-ocean processes and variability.

In another study, it would be interesting to use a more extensive time series to support our findings on a longer time scale. It would also be interesting to study the impact of the LSW formation rate on the North Atlantic basin and how it impacts the North Atlantic overturning.

### Acknowledgments

For access to the model output, visit <http://knossos.eas.ualberta.ca/anha/anhatable.php> website. We gratefully acknowledge the financial and logistic support of grants from the Natural Sciences and Engineering Research Council (NSERC) of Canada (RGPIN 04357 and RGPC 433898). We are grateful to the NEMO development team and the Drakkar project for providing the model and continuous guidance, and to Westgrid and Compute Canada for computational resources. We would also like to thank G. Smith for the CGRF forcing fields, made available by Environment and Climate Change Canada, and G. Garric for the GLORYS2v3 output. Greenland freshwater flux data analyzed in this study is that presented in Bamber et al. (2012) and is available on request as a gridded product. The authors also acknowledge the use of the ARIANE Lagrangian tool (<http://stockage.univ-brest.fr/~grima/Ariane>).

### References

- Bamber, J., van den Broeke, M., Ettema, J., Lenaerts, J., & Rignot, E. (2012). Recent large increases in freshwater fluxes from Greenland into the North Atlantic. *Geophysical Research Letters*, *39*, L19501. <https://doi.org/10.1029/2012GL052552>
- Barnier, B., Madec, G., Penduff, T., Molines, J.-M., Treguier, A.-M., Le Sommer, J., et al. (2006). Impact of partial steps and momentum advection schemes in a global ocean circulation model at eddy-permitting resolution. *Ocean Dynamics*, *56*(5), 543–567. <https://doi.org/10.1007/s10236-006-0082-1>
- Blanke, B., Arhan, M., Lazar, A., & Prévost, G. (2002). A Lagrangian numerical investigation of the origins and fates of the salinity maximum water in the Atlantic. *Journal of Geophysical Research*, *107*(C10), 3163. <https://doi.org/10.1029/2002JC001318>
- Blanke, B., Arhan, M., Madec, G., & Roche, S. (1999). Warm water paths in the equatorial Atlantic as diagnosed with a General Circulation Model. *Journal of Physical Oceanography*, *29*(11), 2753–2768. [https://doi.org/10.1175/1520-0485\(1999\)29029<2753%3AWWPITE>2.0.CO;3B2](https://doi.org/10.1175/1520-0485(1999)29029<2753%3AWWPITE>2.0.CO;3B2)
- Blanke, B., & Raynaud, S. (1997). Kinematics of the Pacific Equatorial Undercurrent: An Eulerian and Lagrangian Approach from GCM Results. *Journal of Physical Oceanography*, *27*(6), 1038–1053. [https://doi.org/10.1175/1520-0485\(1997\)027<1038:KOTPEU>2.0.CO;2](https://doi.org/10.1175/1520-0485(1997)027<1038:KOTPEU>2.0.CO;2)
- Böning, C. W., Behrens, E., Biastoch, A., Getzlaff, K., & Bamber, J. L. (2016). Emerging impact of Greenland meltwater on deepwater formation in the North Atlantic Ocean. *Nature Geoscience*, *9*, 523–527. Retrieved from <https://doi.org/10.1038/ngeo2740>
- Böning, C. W., Scheinert, M., Dengg, J., Biastoch, A., & Funk, A. (2006). Decadal variability of subpolar gyre transport and its reverberation in the North Atlantic overturning. *Geophysical Research Letters*, *33*, L21S01. <https://doi.org/10.1029/2006GL026906>
- Bouillon, S., Morales Maqueda, M. Á., Legat, V., & Fichet, T. (2009). An elastic-viscous-plastic sea ice model formulated on Arakawa B and C grids. *Ocean Modelling*, *27*(3), 174–184. <https://doi.org/10.1016/j.ocemod.2009.01.004>
- Chanut, J., Barnier, B., Large, W., Debreu, L., Penduff, T., Molines, J. M., & Mathiot, P. (2008). Mesoscale eddies in the Labrador Sea and their contribution to convection and restratification. *Journal of Physical Oceanography*, *38*(8), 1617–1643. <https://doi.org/10.1175/2008JPO3485.1>
- Clarke, R. A., & Gascard, J.-C. (1983). The formation of Labrador Sea Water. Part I: Large-scale processes. *Journal of Physical Oceanography*, *13*(10), 1764–1778. [https://doi.org/10.1175/1520-0485\(1983\)013<1764:TFOLSW>2.0.CO;2](https://doi.org/10.1175/1520-0485(1983)013<1764:TFOLSW>2.0.CO;2)
- Courtois, P., Garcia, Y., Hu, X., & Myers, P. G. (2018). Kinematic Subduction Rate of Labrador Sea Water. (Under review).
- Courtois, P., Hu, X., Pennelly, C., Spence, P., & Myers, P. G. (2017). Mixed layer depth calculation in deep convection regions in ocean numerical models. *Ocean Modelling*, *120*, 60–78. <https://doi.org/10.1016/j.ocemod.2017.10.007>
- Cushman-Roisin, B. (1987). Subduction, dynamics of the oceanic surface mixed layer (pp. 181–196).
- Daniault, N., Mercier, H., Lherminier, P., Sarafanov, A., Falina, A., Zunino, P., et al. (2016). The northern North Atlantic Ocean mean circulation in the early 21st century. *Progress in Oceanography*, *146*, 142–158. <https://doi.org/10.1016/j.pocean.2016.06.007>
- Dengler, M., Schott, F. A., Eden, C., Brandt, P., Fischer, J., & Zantopp, R. J. (2004). Break-up of the Atlantic Deep Western Boundary Current into eddies at 8°S. *Nature*, *432*(7020), 1018–1020. <https://doi.org/10.1038/nature03134>
- Dickson, R. R., & Brown, J. (1994). The production of North Atlantic Deep Water: Sources, rates, and pathways. *Journal of Geophysical Research*, *99*(C6), 12,319–12,341. <https://doi.org/10.1029/94JC00530>
- Dickson, R. R., Lazier, J., Meincke, J., Rhines, P., & Swift, J. (1996). Long-term coordinated changes in the convective activity of the North Atlantic. *Progress in Oceanography*, *38*(3), 241–295. [https://doi.org/10.1016/S0079-6611\(97\)00002-5](https://doi.org/10.1016/S0079-6611(97)00002-5)
- Fichet, T., & Morales Maqueda, M. A. (1997). Sensitivity of a global sea ice model to the treatment of ice thermodynamics and dynamics. *Journal of Geophysical Research*, *102*(C6), 12,609–12,646. <https://doi.org/10.1029/97JC00480>
- Fischer, J., & Schott, F. A. (2002). Labrador Sea Water tracked by profiling floats—From the boundary current into the Open North Atlantic. *Journal of Physical Oceanography*, *32*(2), 573–584. [https://doi.org/10.1175/1520-0485\(2002\)032<0573:LSWTBP>2.0.CO;2](https://doi.org/10.1175/1520-0485(2002)032<0573:LSWTBP>2.0.CO;2)
- Fröb, F., Olsen, A., Våge, K., Moore, G. W. K., Yashayaev, I., Jeansson, E., & Rajasakaren, B. (2016). Irminger sea deep convection injects oxygen and anthropogenic carbon to the ocean interior. *Nature Communications*, *7*, 13244. <https://doi.org/10.1038/ncomms13244>
- Grivault, N., Hu, X., & Myers, P. G. (2018). Impact of the surface stress on the volume and freshwater transport through the Canadian Arctic archipelago from a high-resolution numerical simulation. *Journal of Geophysical Research: Oceans*, *123*, 9038–9060. <https://doi.org/10.1029/2018JC013984>
- Häkkinen, S., & Rhines, P. B. (2004). Decline of subpolar North Atlantic circulation during the 1990s. *Science*, *304*(5670), 555. <https://doi.org/10.1126/science.1094917>
- Handmann, P., Fischer, J., Visbeck, M., Johannes, K., Arne, B., Böning, C., & Patara, L. (2018). The Deep Western Boundary Current in the Labrador Sea from observations and a high-resolution model. *Journal of Geophysical Research: Oceans*, *123*, 2829–2850. <https://doi.org/10.1002/2017JC013702>

- Hirschi, J., & Marotzke, J. (2007). Reconstructing the Meridional Overturning Circulation from boundary densities and the zonal wind stress. *Journal of Physical Oceanography*, 37(3), 743–763. <https://doi.org/10.1175/JPO3019.1>
- Holte, J., & Straneo, F. (2017). Seasonal Overturning of the Labrador Sea as Observed by Argo Floats. *Journal of Physical Oceanography*, 47(10), 2531–2543. <https://doi.org/10.1175/JPO-D-17-0051.1>
- Hu, X., Sun, J., Chan, T. O., & Myers, P. G. (2018). Thermodynamic and dynamic ice thickness contributions in the Canadian Arctic Archipelago in NEMO-LIM2 numerical simulations. *The Cryosphere*, 12(4), 1233–1247. <https://doi.org/10.5194/tc-12-1233-2018>
- Hunke, E. C., & Dukowicz, J. K. (1997). An elastic–viscous–plastic model for sea ice dynamics. *Journal of Physical Oceanography*, 27(9), 1849–1867. [https://doi.org/10.1175/1520-0485\(1997\)027<1849:AEVPMF>2.0.CO;2](https://doi.org/10.1175/1520-0485(1997)027<1849:AEVPMF>2.0.CO;2)
- Kieke, D., & Yashayaev, I. (2015). Studies of Labrador Sea Water formation and variability in the subpolar North Atlantic in the light of international partnership and collaboration. *Progress in Oceanography*, 132, 220–232. <https://doi.org/10.1016/j.pocean.2014.12.010>
- Kuhlbrodt, T., Griesel, A., Montoya, M., Levermann, A., Hofmann, M., & Rahmstorf, S. (2007). On the driving processes of the Atlantic Meridional Overturning Circulation. *Reviews of Geophysics*, 45, RG2001. <https://doi.org/10.1029/2004RG000166>
- Lavender, K. L., Davis, R. E., & Owens, W. B. (2000). Mid-depth recirculation observed in the interior Labrador and Irminger seas by direct velocity measurements. *Nature*, 407(6800), 66–69. <https://doi.org/10.1038/35024048>
- Li, F., & Lozier, M. S. (2018). On the linkage between Labrador Sea Water volume and overturning circulation in the Labrador Sea: A case study on proxies. *Journal of Climate*, 31(13), 5225–5241. <https://doi.org/10.1175/JCLI-D-17-0692.1>
- Lozier, M. S., Bacon, S., Bower, A. S., Cunningham, S. A., de Jong, M. F., de Steur, L., et al. (2016). Overturning in the Subpolar North Atlantic Program: A new international ocean observing system. *Bulletin of the American Meteorological Society*, 98, 737–752. <https://doi.org/10.1175/BAMS-D-16-0057.1>
- Lozier, M. S., Gary, S. F., & Bower, A. S. (2012). Simulated pathways of the overflow waters in the North Atlantic: Subpolar to subtropical export. *Deep Sea Research Part II: Topical Studies in Oceanography*, 85, 147–153. <https://doi.org/10.1016/j.dsr2.2012.07.037>
- Lozier, M. S., Li, F., Bacon, S., Bahr, F., Bower, A. S., Cunningham, S. A., et al. (2019). A sea change in our view of overturning in the subpolar North Atlantic. *Science*, 363(6426), 516. <https://doi.org/10.1126/science.aau6592>
- Madec, G. (2008). *Nemo ocean engine, note du pôle de modélisation*, 27. France: Institut Pierre-Simon Laplace (IPSL).
- Marsh, R., de Cuevas, B. A., Coward, A. C., Bryden, H. L., & Alvarez, M. (2005). Thermohaline circulation at three key sections in the North Atlantic over 1985–2002. *Geophysical Research Letters*, 32, L10604. <https://doi.org/10.1029/2004GL022281>
- Marshall, J. C., Williams, R. G., & Nurser, A. J. G. (1993). Inferring the subduction rate and period over the North Atlantic. *Journal of Physical Oceanography*, 23(7), 1315–1329. [https://doi.org/10.1175/1520-0485\(1993\)023<1315:ITSRAP>2.0.CO;2](https://doi.org/10.1175/1520-0485(1993)023<1315:ITSRAP>2.0.CO;2)
- Masina, S., Storto, A., Ferry, N., Valdivieso, M., Haines, K., Balmaseda, M., et al. (2015). An ensemble of eddy-permitting global ocean reanalyses from the MyOcean project. *Climate Dynamics*, 49(3), 813–841. <https://doi.org/10.1007/s00382-015-2728-5>
- Mauritzen, C., & Häkkinen, S. (1999). On the relationship between dense water formation and the “Meridional Overturning Cell” in the North Atlantic Ocean. *Deep Sea Research Part I: Oceanographic Research Papers*, 46(5), 877–894. [https://doi.org/10.1016/S0967-0637\(98\)00094-6](https://doi.org/10.1016/S0967-0637(98)00094-6)
- McCarthy, G. D., Smeed, D. A., Johns, W. E., Frajka-Williams, E., Moat, B. I., Rayner, D., et al. (2015). Measuring the Atlantic Meridional Overturning Circulation at 26° N. *Progress in Oceanography*, 130, 91–111. <https://doi.org/10.1016/j.pocean.2014.10.006>
- Pickart, R. S., & Spall, M. A. (2007). Impact of Labrador Sea convection on the North Atlantic Meridional Overturning Circulation. *Journal of Physical Oceanography*, 37(9), 2207–2227. <https://doi.org/10.1175/JPO3178.1>
- Pickart, R. S., Spall, M. A., & Lazier, John R. N. (1997). Mid-depth ventilation in the western boundary current system of the sub-polar gyre. *Deep Sea Research Part I: Oceanographic Research Papers*, 44(6), 1025–1054. [https://doi.org/10.1016/S0967-0637\(96\)00122-7](https://doi.org/10.1016/S0967-0637(96)00122-7)
- Piron, A., Thierry, V., Mercier, H., & Caniaux, G. (2016). Argo float observations of basin-scale deep convection in the Irminger sea during winter 2011–2012. *Deep Sea Research Part I: Oceanographic Research Papers*, 109, 76–90. <https://doi.org/10.1016/j.dsr.2015.12.012>
- Rattan, S., Myers, P. G., Treguier, A.-M., Theetten, S., Biastoch, A., & Böning, C. (2010). Towards an understanding of Labrador Sea salinity drift in eddy-permitting simulations. *Ocean Modelling*, 35(1), 77–88. <https://doi.org/10.1016/j.ocemod.2010.06.007>
- Rhein, M., Kieke, D., Hüttl-Kabus, S., Roessler, A., Mertens, C., Meissner, R., & Yashayaev, I. (2011). Deep water formation, the subpolar gyre, and the Meridional Overturning Circulation in the subpolar North Atlantic. *Deep Sea Research Part II: Topical Studies in Oceanography*, 58(17), 1819–1832. <https://doi.org/10.1016/j.dsr2.2010.10.061>
- Rhein, M., Steinfeldt, R., Kieke, D., Stendero, I., & Yashayaev, I. (2017). Ventilation variability of Labrador Sea Water and its impact on oxygen and anthropogenic carbon: a review. *Philosophical Transactions of the Royal Society of London A: Mathematical, Physical and Engineering Sciences*, 375(2102). <https://doi.org/10.1098/rsta.2016.0321>
- Smith, G. C., Roy, F., Mann, P., Dupont, F., Brasnett, B., Lemieux, J.-F., et al. (2014). A new atmospheric dataset for forcing ice–ocean models: Evaluation of reforecasts using the Canadian global deterministic prediction system. *Quarterly Journal of the Royal Meteorological Society*, 140(680), 881–894. <https://doi.org/10.1002/qj.2194>
- Straneo, F. (2006). On the connection between dense water formation, overturning, and poleward heat transport in a convective basin. *Journal of Physical Oceanography*, 36(9), 1822–1840. <https://doi.org/10.1175/JPO2932.1>
- Straneo, F., Pickart, R. S., & Lavender, K. (2003). Spreading of Labrador sea water: An advective-diffusive study based on Lagrangian data. *Deep-Sea Research Part I-Oceanographic Research Papers*, 50(6), 701–719. [https://doi.org/10.1016/S0967-0637\(03\)00057-8](https://doi.org/10.1016/S0967-0637(03)00057-8)
- Talley, L. D., & McCartney, M. S. (1982). Distribution and circulation of Labrador Sea Water. *Journal of Physical Oceanography*, 12(11), 1189–1205. [https://doi.org/10.1175/1520-0485\(1982\)012<1189:DACOLS>2.0.CO;2](https://doi.org/10.1175/1520-0485(1982)012<1189:DACOLS>2.0.CO;2)
- Thornalley, D. J. R., Oppo, D. W., Ortega, P., Robson, J. I., Brierley, C. M., Davis, R., et al. (2018). Anomalously weak Labrador Sea convection and Atlantic overturning during the past 150 years. *Nature*, 556(7700), 227–230. <https://doi.org/10.1038/s41586-018-0007-4>
- Toole, J., Curry, R. G., Joyce, T. M., McCartney, M., & Peña-Molino, B. (2011). Transport of the North Atlantic Deep Western Boundary Current about 39° N, 70° W: 2004–2008. *Deep Sea Research Part II: Topical Studies in Oceanography*, 58(17), 1768–1780.
- Toole, J., Magdalena, A., Le Bras, I. A., Joyce, T. M., & McCartney, M. S. (2017). Moored observations of the Deep Western Boundary Current in the NW Atlantic: 2004–2014. *Journal of Geophysical Research: Oceans*, 122, 7488–7505. <https://doi.org/10.1002/2017JC012984>
- Williams, R. (2001). Ocean subduction. *Management*, 25(1), 1982–1993.
- Yashayaev, I. (2007). Hydrographic changes in the Labrador Sea, 1960–2005. *Progress in Oceanography*, 73(3–4), 242–276. <https://doi.org/10.1016/j.pocean.2007.04.015>
- Yashayaev, I., Bersch, M., & van Aken, H. M. (2007). Spreading of the Labrador Sea Water to the Irminger and Iceland basins. *Geophysical Research Letters*, 34, L10602. <https://doi.org/10.1029/2006GL028999>
- Yashayaev, I., & Loder, J. W. (2009). Enhanced production of Labrador Sea Water in 2008. *Geophysical Research Letters*, 36, L01606. <https://doi.org/10.1029/2008GL036162>
- Yashayaev, I., & Loder, J. W. (2016). Recurrent replenishment of Labrador Sea Water and associated decadal-scale variability. *Journal of Geophysical Research: Oceans*, 121, 8095–8114. <https://doi.org/10.1002/2016JC012046>



- Yashayaev, I., & Loder, J. W. (2017). Further intensification of deep convection in the Labrador Sea in 2016. *Geophysical Research Letters*, *44*, 1429–1438. <https://doi.org/10.1002/2016GL071668>
- Yashayaev, I., van Aken, H. M., Holliday, N. P., & Bersch, M. (2007). Transformation of the Labrador Sea Water in the subpolar North Atlantic. *Geophysical Research Letters*, *34*, L22605. <https://doi.org/10.1029/2007GL031812>
- Zantopp, R., Fischer, J., Visbeck, M., & Karstensen, J. (2017). From interannual to decadal—17 years of boundary current transports at the exit of the Labrador Sea. *Journal of Geophysical Research: Oceans*, *122*, 1724–1748. <https://doi.org/10.1002/2016JC012271>
- Zou, S., & Lozier, M. S. (2016). Breaking the linkage between Labrador Sea water production and its advective export to the subtropical gyre. *Journal of Physical Oceanography*, *46*(7), 2169–2182. <https://doi.org/10.1175/JPO-D-15-0210.1>